Dear Author

Please use this PDF proof to check the layout of your article. If you would like any changes to be made to the layout, you can leave instructions in the online proofing interface. Making your changes directly in the online proofing interface is the quickest, easiest way to correct and submit your proof. Please note that changes made to the article in the online proofing interface will be added to the article before publication, but are not reflected in this PDF proof.

If you would prefer to submit your corrections by annotating the PDF proof, please download and submit an annotatable PDF proof by clicking here and you'll be redirected to our PDF Proofing system.

Nanoscale d0nr04246c

We have presented the graphical abstract image and text for your article below. This briefly summarises your work, and will be presented with your article online.

1

A new route for the shape differentiation of cesium lead bromide perovskite nanocrystals with near-unity photoluminescence quantum yield

Roberto Grisorio,* Daniele Conelli, Rosa Giannelli, Elisabetta Fanizza, Marinella Striccoli, Davide Altamura, Cinzia Giannini, Ignazio Allegretta, Roberto Terzano and Gian Paolo Suranna

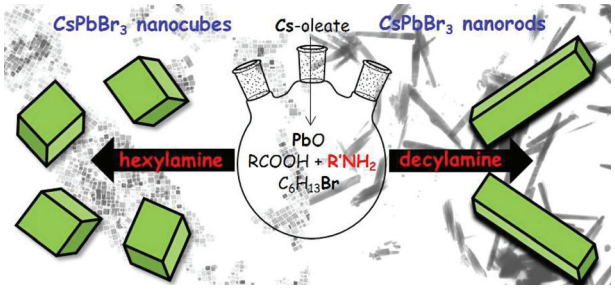

Engineering the chemical approach for obtaining cesium lead bromide perovskite nanocrystals allows their shape modulation while maintaining their near-unity photoluminescence quantum yield.

Please check this proof carefully. Our staff will not read it in detail after you have returned it.

Please send your corrections either as a copy of the proof PDF with electronic notes attached or as a list of corrections. **Do not edit the text within the PDF or send a revised manuscript** as we will not be able to apply your corrections. Corrections at this stage should be minor and not involve extensive changes.

Proof corrections must be returned as a single set of corrections, approved by all co-authors. No further corrections can be made after you have submitted your proof corrections as we will publish your article online as soon as possible after they are received.

Please ensure that:

- The spelling and format of all author names and affiliations are checked carefully. You can check how we have identified the authors' first and last names in the researcher information table on the next page. **Names will be indexed and cited as shown on the proof, so these must be correct.**
- Any funding bodies have been acknowledged appropriately and included both in the paper and in the funder information table on the next page.
- All of the editor's queries are answered.
- Any necessary attachments, such as updated images or ESI files, are provided.

Translation errors can occur during conversion to typesetting systems so you need to read the whole proof. In particular please check tables, equations, numerical data, figures and graphics, and references carefully.

Please return your **final** corrections, where possible within **48 hours** of receipt following the instructions in the proof notification email. If you require more time, please notify us by email to nanoscale@rsc.org.

Funding information

Providing accurate funding information will enable us to help you comply with your funders' reporting mandates. Clear acknowledgement of funder support is an important consideration in funding evaluation and can increase your chances of securing funding in the future.

We work closely with Crossref to make your research discoverable through the Funding Data search tool (http://search.crossref.org/funding). Funding Data provides a reliable way to track the impact of the work that funders support. Accurate funder information will also help us (i) identify articles that are mandated to be deposited in **PubMed Central (PMC)** and deposit these on your behalf, and (ii) identify articles funded as part of the **CHORUS** initiative and display the Accepted Manuscript on our web site after an embargo period of 12 months.

Further information can be found on our webpage (http://rsc.li/funding-info).

What we do with funding information

We have combined the information you gave us on submission with the information in your acknowledgements. This will help ensure the funding information is as complete as possible and matches funders listed in the Crossref Funder Registry.

If a funding organisation you included in your acknowledgements or on submission of your article is not currently listed in the registry it will not appear in the table on this page. We can only deposit data if funders are already listed in the Crossref Funder Registry, but we will pass all funding information on to Crossref so that additional funders can be included in future.

Please check your funding information

The table below contains the information we will share with Crossref so that your article can be found *via* the Funding Data search tool. **Please check that the funder names and grant numbers in the table are correct and indicate if any changes are necessary to the Acknowledgements text.**

Funder name	Funder's main country of origin	Funder ID (for RSC use only)	Award/grant number
Regione Puglia	Italy	501100009886	Y8V9H90-1

Researcher information

Please check that the researcher information in the table below is correct, including the spelling and formatting of all author names, and that the authors' first, middle and last names have been correctly identified. **Names will be indexed and cited as shown on the proof, so these must be correct.**

If any authors have ORCID or ResearcherID details that are not listed below, please provide these with your proof corrections. Please ensure that the ORCID and ResearcherID details listed below have been assigned to the correct author. Authors should have their own unique ORCID iD and should not use another researcher's, as errors will delay publication.

Please also update your account on our online manuscript submission system to add your ORCID details, which will then be automatically included in all future submissions. See here for step-by-step instructions and more information on author identifiers.

First (given) and middle name(s)	Last (family) name(s)	ResearcherID	ORCID iD
Roberto	Grisorio		0000-0002-3698-9370
Daniele	Conelli		
Rosa	Giannelli		
Elisabetta	Fanizza		0000-0001-6293-9388
Marinella	Striccoli		0000-0002-5366-691X
Davide	Altamura		
Cinzia	Giannini		
Ignazio	Allegretta		

Roberto	Terzano		
Gian Paolo	Suranna		

Queries for the attention of the authors

Journal: **Nanoscale** Paper: **d0nr04246c**

Title: **A new route for the shape differentiation of cesium lead bromide perovskite nanocrystals with near-unity photoluminescence quantum yield**

For your information: You can cite this article before you receive notification of the page numbers by using the following format: (authors), Nanoscale, (year), DOI: 10.1039/d0nr04246c.

Editor's queries are marked like this Q1, Q2, and for your convenience line numbers are indicated like this 5, 10, 15, ...

Please ensure that all queries are answered when returning your proof corrections so that publication of your article is not delayed.

Query Reference	Query	Remarks
Q1	Please confirm that the spelling and format of all author names is correct. Names will be indexed and cited as shown on the proof, so these must be correct. No late corrections can be made.	
Q2	The sentence beginning "This approach warrants ..." has been altered for clarity. Please check that the meaning is correct.	
Q3	The meaning of the phrase "The last were confirmed" in the sentence beginning "The last were ..." is not clear. Please provide alternative text.	
Q4	In the sentence beginning "To a 50 mL Schlenk tube..." and elsewhere in the manuscript, please check that "0. g" has been presented correctly.	
Q5	Ref. 23: Please check that the last name for the 3rd author is displayed correctly.	
Q6	Ref. 34: Please check that the last names for the 3rd and 4th authors are displayed correctly.	
Q7	Ref. 46: Please check that the last name for the 7th author is displayed correctly.	

Nanoscale

PAPER

A new route for the shape differentiation of cesium lead bromide perovskite nanocrystals with near-unity photoluminescence quantum yield†

Cite this: DOI: 10.1039/d0nr04246c

Roberto Grisorio, *[a] Daniele Conelli,[a] Rosa Giannelli,[a] Elisabetta Fanizza, [b,c] Marinella Striccoli, [c] Davide Altamura,[d] Cinzia Giannini,[d] Ignazio Allegretta,[e] Roberto Terzano[e] and Gian Paolo Suranna[a,f]

The ongoing interest in all-inorganic cesium lead bromide perovskite nanocrystals ($CsPbBr_3$ NCs) is mainly due to their optical properties, in particular their high photoluminescence quantum yields (PLQYs). Three-precursor synthetic methods, in which the sources of the three elements (cesium, lead and bromine) constituting the perovskite scaffold are chemically independent, often succeed in the achievement of near-unity PLQY perovskite NCs. However, this class of synthetic approaches precludes the accessibility to crystal morphologies different from the traditional cuboidal ones. In order to upgrade three-precursor synthetic schemes to obtain more sophisticated morphologies – such as the rods – we propose a conceptually original synthetic methodology, in which a potentially controllable stage of the reaction anticipates the fast crystallization promoted by cesium injection. To this purpose, lead oxide, 1-bromohexane (at different molar ratios with respect to lead) and the ligands (oleic acid and a suitable amine) in 1-octadecene are reacted at 160 °C for an incubation period of 30 min before cesium injection. During this stage, and at high $C_6H_{13}Br$/PbO molar ratios, the bromide release from reactions between the ligands and 1-bromohexane promotes the evolution of $[PbBr_{(2+n)}]^{n-}$ species as well as of two-dimensional $[(RNH_3)_2(PbBr_4)]_n$ structures a rod-like shape (aspect ratios ~10). These structures act as the templating agents for the subsequent crystallization promoted by cesium injection, ensuring the formation of near-unity PLQY nanorods in the presence of decylamine. Conversely, the pronounced decomposition of the preformed $[(RNH_3)_2(PbBr_4)]_n$ structures preludes the formation of near-unity PLQY nanocubes in the presence of hexylamine. The amine choice exerts also an important role in the emission stability of the corresponding NCs, since the nanocubes prepared in the presence of hexylamine maintain their near-unity PLQYs up to 90 days under ambient conditions. In addition to the long-term PLQY stability, the nanorods prepared with decylamine also exhibit a remarkable resistance to the presence of water, due to a compact and hydrophobic organic shell passivating the NC surface. These findings can contribute to the development of innovative synthetic methodologies for controlling the shape and stability of near-unity PLQY perovskite NCs.

Received 3rd June 2020,
Accepted 17th July 2020

DOI: 10.1039/d0nr04246c

rsc.li/nanoscale

[a]Dipartimento di Ingegneria Civile, Ambientale, del Territorio, Edile e di Chimica (DICATECh), Politecnico di Bari, Via Orabona 4, 70125 Bari, Italy. E-mail: roberto.grisorio@poliba.it
[b]Dipartimento di Chimica, Università degli Studi di Bari "Aldo Moro", Via Orabona 4, 70126 Bari, Italy
[c]CNR – Istituto per i Processi Chimico Fisici, UOS Bari, Via Orabona 4, 70126 Bari, Italy
[d]CNR – Istituto di Cristallografia, via Amendola 122/O, Bari 70126, Italy
[e]Dipartimento di Scienze del Suolo, della Pianta e degli Alimenti, Università degli Studi di Bari "Aldo Moro", Via G. Amendola 165/A, 70126 Bari, Italy
[f]CNR NANOTEC – Istituto di Nanotecnologia, Via Monteroni, 73100 Lecce, Italy

†Electronic supplementary information (ESI) available: Tables reporting the reaction conditions and optical properties of the NCs synthesized for this studies. Additional spectroscopic investigations: UV-vis spectra, NMR spectra and TEM images. See DOI: 10.1039/d0nr04246c

Introduction

Lead halide perovskite nanocrystals (NCs) continue to receive great attention from the scientific community due to their high potential in different technological fields spanning from lighting[1,2] to photovoltaics.[3] Among the various lead halide perovskite NCs, all-inorganic $CsPbBr_3$ nanoparticles[4] are being deeply investigated for their narrow emission line widths and potential near-unity photoluminescence quantum yields (PLQYs).[5] However, the structural stability of lead halide perovskite NCs is undermined by weak bonds between their chemical constituents, exposing them to the formation of defects.[6,7] As a result, concerns are raised about the long-term

stability of $CsPbBr_3$ NCs,[8] which is generally compromised by the dynamic nature of their surface passivation[9–11] as well as by the complexity of their organic/inorganic interfaces.[12,13] Regarding their crystalline defects, the most recurrent ones for lead halide perovskite NCs are halide vacancies, which activate the non-radiative pathways for the excited states in nanoparticles.[14,15] For these reasons, relatively low PLQYs (50–80%) are typically obtained for samples prepared under lead-rich synthetic conditions dictated by the use of $PbBr_2$ species as both the lead and halide source (the so-called two-precursor method).[16,17] Conversely, the three-precursor approach utilizes alternative bromide sources (such as *N*-bromosuccinimide,[18] benzoyl bromide,[19] trimethylsilyl bromide,[20] TOP-Br_2,[21] alkyl-ammonium bromides[22,23] or ionic liquids[24]) and is chemically independent of the lead precursor, commonly lead acetate or lead oxide. This approach warrants the agreement of the theoretical stoichiometric ratio between the individual elements composing the perovskite structure, a requisite for the potential achievement of near-unity PLQY emissive nanoparticles.[25,26] To date, however, its main limitation regards the achievement of highly emissive nanoparticles endowed with morphologies (such as nanorods) more sophisticated than that of the traditional nanocubes. This drawback originates from the lack of fundamental knowledge required for the morphological control of the relevant perovskite NCs prepared by the three-precursor approach. Commonly, the assembly of anisotropic $CsPbBr_3$ NCs necessitates peculiar reaction conditions[27–29] or slow reaction kinetics,[30,31] which might not be compatible with the effective circumstances generating highly luminescent NCs.[32]

In order to circumvent this limitation, in this study we propose a conceptually original synthetic approach, in which a potentially controllable stage of the reaction anticipates the fast crystallization promoted by cesium injection. To this purpose, a mixture of lead oxide, 1-bromohexane and the ligands (oleic acid and the suitable amine) in 1-octadecene was incubated for 30 min before the injection of a warm cesium oleate solution[33] (Scheme 1). The release of bromide anions[34] (due to SN_2 reactions between the ligands and the aliphatic halide) under peculiar reaction conditions allowed the morphological control of the formed rod-like $[(RNH_3)_2(PbBr_4)]_n$ structures, which partially retained their shape, acting as templating agents for the subsequent nanocrystal growth promoted by cesium injection. By suitably modulating the organic ligand composition and the combination of the perovskite elements, this synthetic methodology enabled the obtainment of near-unity PLQY and stable $CsPbBr_3$ nanorods, near-unity PLQY nanocubes with different dimensions and pure Cs_4PbBr_6 nanoparticles.

Results and discussion

To appropriately exploit the potential of the proposed synthetic approach for obtaining $CsPbBr_3$ NCs, the first step was to analyze carefully the reaction mixture before the injection of

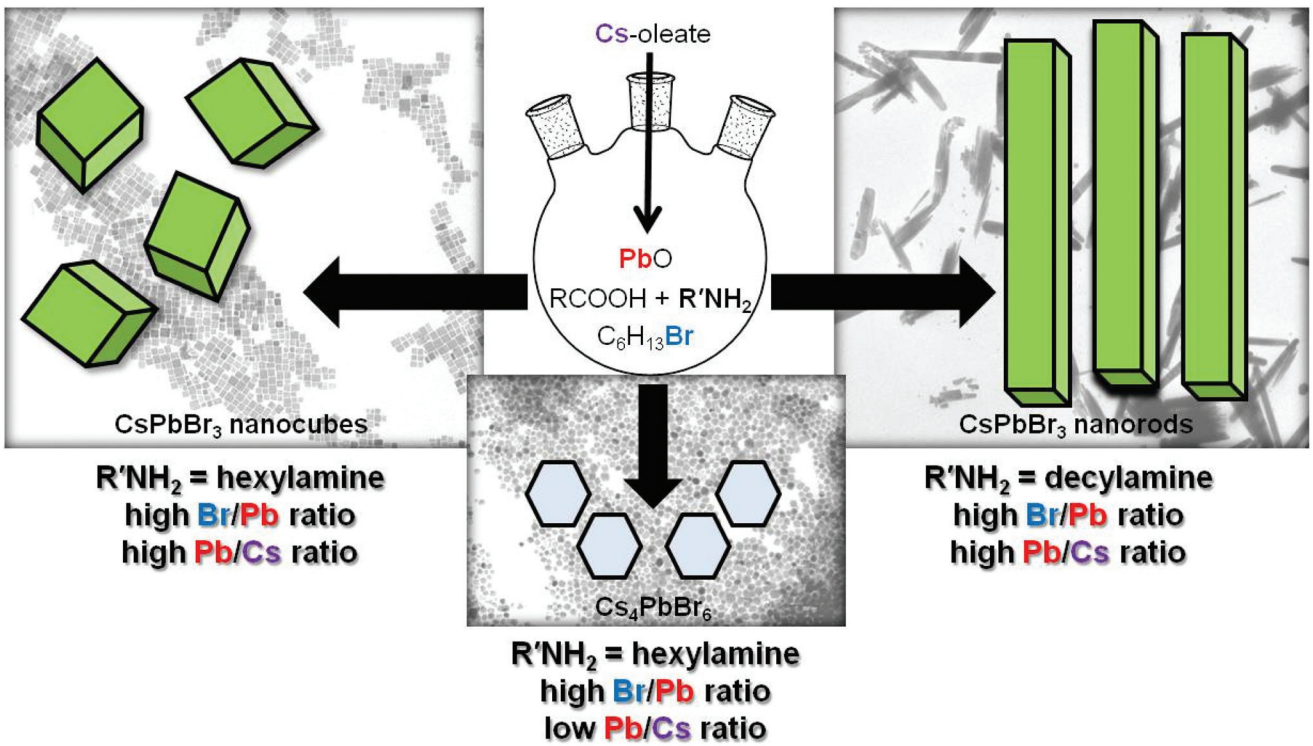

Scheme 1 Schematic representation of the synthetic protocol adopted for obtaining near-unity PLQY and stable $CsPbBr_3$ NCs and Cs_4PbBr_6 NCs in the presence of 1-bromohexane as the halide source.

the cesium source, *i.e.* the solution obtained by mixing lead oxide, oleic acid, oleylamine (OAM) and 1-bromohexane (from 3.0 to 6.0 equivalents with respect to lead) in 1-octadecene at 160 °C for a predetermined incubation time (30 min). The ^{1}H-NMR characterization of the mixtures at different $C_6H_{13}Br$/PbO molar ratios evidenced the formation of an ester and a secondary amine (Fig. 1A), which are released as side products of the SN_2 reactions between 1-bromohexane and the ligands, generating the bromide ions necessary for the perovskite structure assembly (top left equations in Fig. 1). It is worth noting how the validity of the proposed synthetic methodology is also based on the fact that these side-products are ineffective as passivating agents of the NC surface.[35,36] In order to estimate approximately the bromide availability in the reaction mixture at the end of the incubation time, we compared the integrals of the specific proton signals ascribable to the secondary and primary amines. We observed a proportionality between this signal ratio and the initial $C_6H_{13}Br$/PbO molar ratio, thus confirming a correlation with the bromide availability at the end of the incubation period. The UV-vis spectroscopic monitoring of the reaction course using 3.0 equivalents of 1-bromohexane with respect to lead oxide revealed the bromide complexation of Pb^{2+} ions released by the formed lead oleate[37] (top right equations in Fig. 1). In fact, the appearance of a broad absorption band (located between 260 and 325 nm), which is absent in the initial stage of the reaction, was consistent with the formation of bromoplumbate species (prevalently $PbBr_2$ and $PbBr_3^-$),[38] while its temporal evolution confirmed the slow release of bromide anions in the reaction mixture. The absorption tail at longer wavelength suggests also the plausible formation of highly coordinated bromoplumbate species ($PbBr_5^{3-}$ and $PbBr_6^{4-}$) which is in agreement with the absorption at 313 nm associated with the isolated $PbBr_6$ octahedra of the 0D trigonal phase (Cs_4PbBr_6).[39] The amount of these species became prevalent upon increasing the $C_6H_{13}Br$/PbO molar ratio (from 4/1 to 6/1) as confirmed by the red-shift of the absorption profile of the corresponding reaction mixtures (Fig. 1C). In these cases, the scenario was completed by the formation of hybrid organic–inorganic two-dimensional structures with the general formula $[(RNH_3)_2(PbBr_4)]_n$, which are

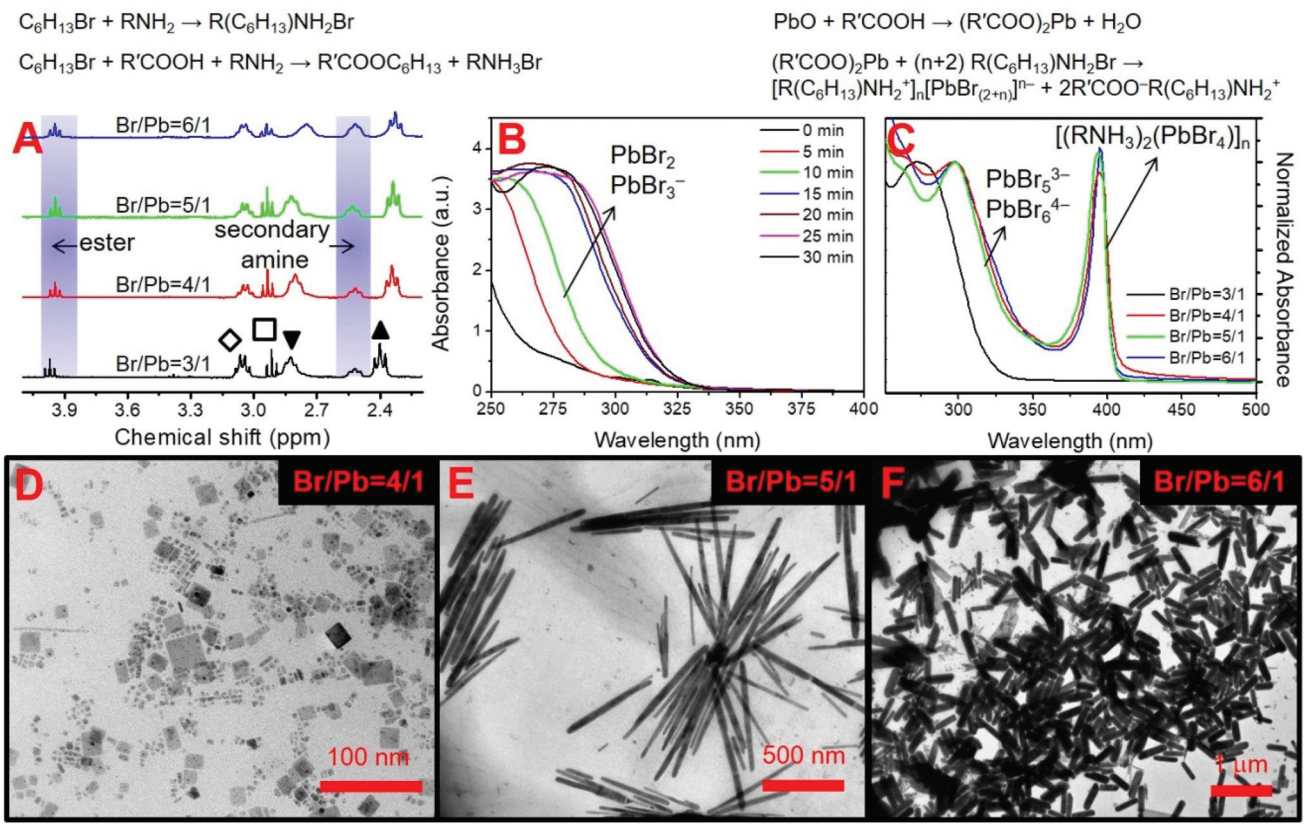

Fig. 1 Top: Reactions occurring during the incubation time before cesium injection; top left: SN_2 reactions generating Br^- ions; top right: generation of Pb^{2+} ions and subsequent formation of bromoplumbate species. (A) ^{1}H-NMR spectra (benzene-d_6) of the mixtures containing lead oxide, oleic acid, oleylamine and different amounts of 1-bromohexane in 1-octadecene, kept at 160 °C for 30 min. The plot highlights the characteristic resonances of the ester (–CH_2COOCH_2–) and of the secondary amine (–CH_2NH–) protons. The chemical shifts of other species present in the reaction mixture are evidenced: ▲ (–CH_2COOH of oleic acid), ▼ (–CH_2NH_2 of oleylamine), □ (–CH_2Br of residual 1-bromohexane) and ◊ (–CONHCH_2– of the amide). (B) UV-Vis spectra evolution (0 → 30 min) of the mixture obtained using $C_6H_{13}Br$/PbO = 3/1. (C) Comparison between the absorption spectra of the reaction mixture at different $C_6H_{13}Br$/PbO ratios. (D–F) TEM images of the isolated $[(RNH_3)_2(PbBr_4)]_n$ structures at different $C_6H_{13}Br$/PbO molar ratios (4/1 → 6/1) after the incubation time period (30 min).

characterized by a peculiar absorption at 395 nm.[40,41] Their formation is due to relatively high concentration of $PbBr_4^{2-}$ species in the corresponding mixtures.

The isolation of the formed particles under these conditions (see the Experimental section for details) enabled their morphological characterization by transmission electron microscopy (TEM). Square-shaped $[(RNH_3)_2(PbBr_4)]_n$ structures (length < 10 nm) were obtained at relatively low molar ratios ($C_6H_{13}Br$/PbO = 4/1, Fig. 1D), whereas rod-shaped structures were generated under the reaction conditions determined by a higher bromide availability (Fig. 1E and F). In particular, when 6.0 equivalents of 1-bromohexane were used with respect to lead oxide, the length (1.05 ± 0.12 μm) of the rod-shaped structures was remarkably higher than their width (0.11 ± 0.02 μm). The aspect ratio (~10) of these structures was similar to that observed for the particles obtained with $C_6H_{13}Br$/PbO = 5/1. The anisotropic growth of $[(RNH_3)_2PbBr_4]_n$ structures in the case of high $C_6H_{13}Br$/PbO molar ratios can be explained by the uncommon proportion between lead and bromide amounts during the incubation stage. A morphological modulation of $[(RNH_3)_2PbBr_4]_n$ structures was thus achieved by considering, however, that the subsequent cesium injection followed by crystallization could unpredictably lead to further modifications, the crystal formation being simultaneously initiated by nucleation of bromoplumbate species.[42]

On these premises, a systematic modulation of the reaction conditions in terms of the molar proportion between the three constituting elements was carried out with the aim of studying its effect on the emission quality and efficiency, phase purity and morphology of the relevant perovskite NCs (Experimental section). The synthetic conditions were further modulated by modifying the chain length of the aliphatic amine, namely by using oleylamine (OAM), decylamine (DAM) and hexylamine (HAM), as summarized in Tables S1–3.† We realized that the search for the optimal reaction conditions leading to near-unity PLQYs with our protocol requires an appropriate combination of the synthetic variables, and that the task is further complicated by the concomitant formation of the 0D trigonal phase (Cs_4PbBr_6).[43] The synthetic conditions yielding nanoparticles exhibiting a near-unity PLQY without concomitant formation of the 0D-phase (**NP6**, **NP20** and **NP22**) and that resulting in a pure 0D-phase (**NP21**) are described in Table 1 and their spectroscopic, morphological and structural investigations are reported in Fig. 2.

When OAM was used as the base (**NP6**, Table 1), the conditions for achieving a near-unity PLQY with a narrow emission profile (fwhm = 19 nm, Fig. 2A) were found by generating a slight stoichiometric excess of bromide ions with respect to lead and by using a low cesium-to-lead molar ratio, in agreement with the previous studies.[18,19] The optical investigation of the obtained nanoparticles in this set of experiments (**NP1–16**, Fig. S1–4†) evidenced no direct correlation between the PLQY and the $C_6H_{13}Br$/PbO molar ratio. This result suggests that the avoidance of structural defects (*i.e.* halide vacancies) during the building-up of the perovskite structure was independent of the bromide availability.[44,45] In addition, the situation was complicated by the co-formation of Cs_4PbBr_6 NCs (characterized by a distinct peak at 314 nm in their absorption spectrum) at relatively high cesium-to-lead ratios, whereas the formation of layered structures (the so-called 2D structures) was favored at relatively low cesium-to-lead ratios. While the high cesium availability could explain the formation of lead-poor perovskite structures (Cs_4PbBr_6), the competition between cesium and oleylammonium ions for the same lattice sites elucidates the formation of layered structures at relatively low cesium-to-lead molar ratios.[46,47]

To explore the viability of the proposed synthetic route for obtaining more sophisticated morphologies, the effects of the amine length was investigated only under the conditions determined by the highest $C_6H_{13}Br$/PbO molar ratio, while the cesium-to-lead molar ratio was systematically increased from 1/4 up to equimolarity (Tables S2 and S3†). The molar amounts of decylamine (DAM) and hexylamine (HAM) used for OAM were the same. In the case of DAM as the base (**NP17–20**, Table S2†), near-unity PLQYs were achieved with the sample prepared with an equimolar cesium-to-lead ratio (**NP20**, Table 1). Its fluorescence also exhibited a relatively narrow emission profile (fwhm = 18 nm, Fig. 2B). Intriguingly, what clearly emerges from the optical characterization of the NCs synthesized using DAM (Fig. S5, Table S2†) is the presence of the residual $[(RNH_3)_2(PbBr_4)]_n$ structures in **NP17–19** samples, which suggests their active role in the formation process of these nanoparticles. Conversely, in the case of NCs obtained in the presence of HAM (**NP21–24**), we observed the propensity to the formation of the 0D trigonal phase with the exception of **NP22** (Fig. S6, Table S3†). While we were also able to obtain the pure non-emissive Cs_4PbBr_6 NCs (**NP21**, Fig. 2C), a slight increase in the cesium-to-lead molar ratio (up to 1/3) led to the formation of a sample (**NP22**) completely deprived

Table 1 Reaction conditions and properties of the main NCs of this study

Sample	Amine[a]	Cs/Pb	Br/Pb	Shape[b]	Elemental composition[c]	Size (nm)	PL (nm)	fwhm (meV)	PLQY (%)
NP6	OAM	1/3	4/1	Cube	$Cs_{1.2}Pb_{1.0}Br_{2.9}$	7.0 ± 1.0	512	92	~100
NP20	DAM	1/1	6/1	Rod	$Cs_{1.3}Pb_{1.0}Br_{2.3}$	15.2 ± 2.4[d]	510	89	~100
NP21	HAM	1/4	6/1	Rhombohedron	$Cs_{4.4}Pb_{1.0}Br_{5.4}$	17.4 ± 2.5	—	—	—
NP22	HAM	1/3	6/1	Cube	$Cs_{1.2}Pb_{1.0}Br_{3.0}$	13.0 ± 1.5	515	81	95

[a] OAM = oleylamine, DAM = decylamine, and HAM = hexylamine. [b] Obtained by transmission electron microscopy. [c] Measured by energy dispersive X-ray analyses. [d] Nanorod width.

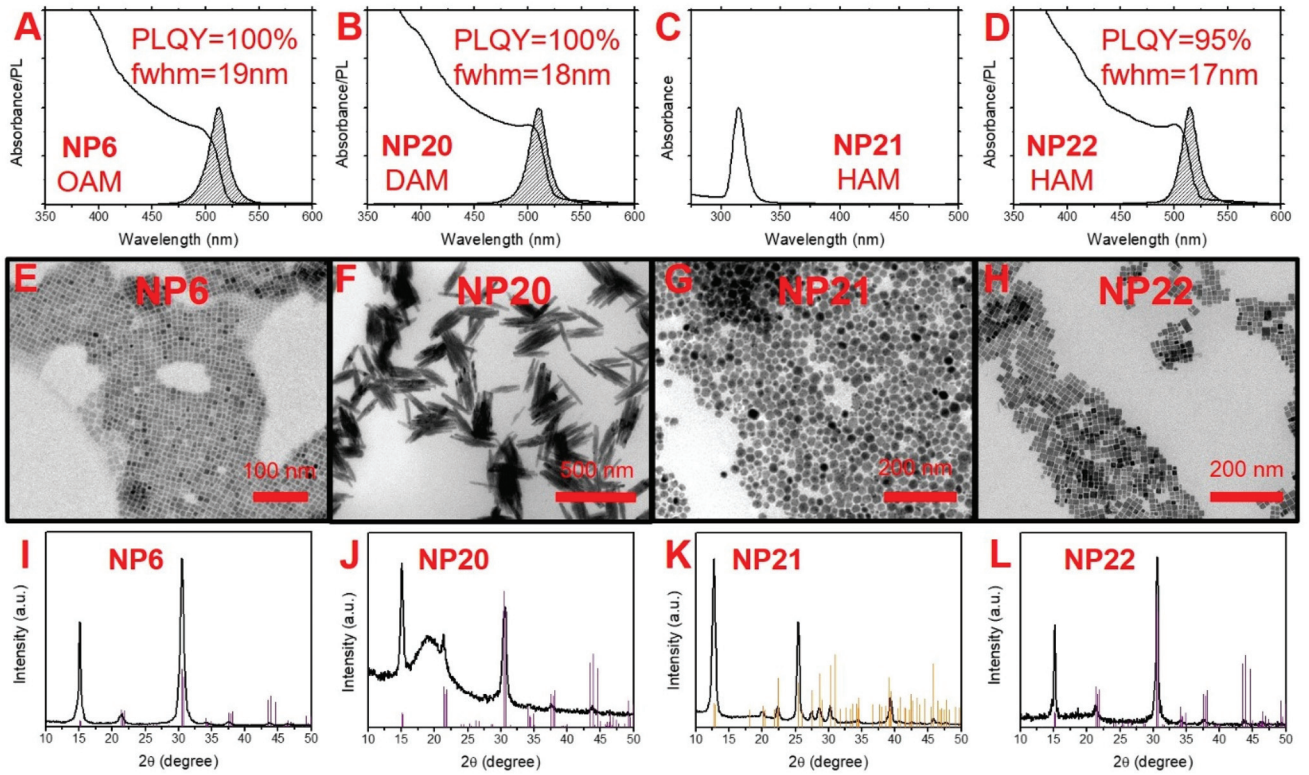

Fig. 2 UV-Vis absorption and PL spectra of **NP6** (A), **NP20** (B), **NP21** (C) and **NP22** (D) recorded in hexane. TEM images of **NP6** (E), **NP20** (F), **NP21** (G) and **NP22** (H). XRD (coupled $\theta/2\theta$ scan) patterns of **NP6** (I), **NP20** (J), **NP21** (K) and **NP22** (L) along with the reference bars for the orthorhombic $CsPbBr_3$ (ICSD-97851) and trigonal Cs_4PbBr_6 (ICSD-25124) phases.

of the trigonal phase; its fluorescence exhibited a relatively narrow emission profile (fwhm = 17 nm, Fig. 2D) with a near-unity PLQY (95%).

Transmission electron microscopy (TEM) measurements revealed the formation of nanorods only in the case of **NP20** (length = 149.9 ± 35.6 nm, width = 15.2 ± 2.4 nm, and aspect ratio = 10), as shown in Fig. 2F. Conversely, we observed the formation of nanocubes in the case of **NP6** and **NP22** (Fig. 2E and H, respectively), with the latter exhibiting larger average sizes (13.0 ± 1.5 nm) than the former (7.0 ± 1.0 nm). The achievement of **NP22** could be interpreted as a benefit for the proposed synthetic protocol, because it is possible to modify the sizes of desired nanocubes while maintaining their near-unity PLQYs. In the case of **NP21**, the morphological characterization confirmed the sole formation of the 0D trigonal phase (Fig. 2G).

The elemental compositions of the samples summarized in Table 1 were investigated by using a field emission gun scanning electron microscopy (FEG-SEM) coupled with energy dispersive X-ray spectroscopy (EDX). The relevant results evidenced that the formal stoichiometry of the $CsPbBr_3$ structure is observed in the case of **NP6** and **NP22**, while the proportion between the elements is in agreement with the formal stoichiometry of the Cs_4PbBr_6 structure in the case of **NP21**. In contrast, the experimental Br/Pb ratio (2.3) strongly suggests a Pb-rich surface of **NP20**, which, at the same time, is yet compatible with high emission efficiencies.[48–50] It is plausible that the Pb-rich surface is a consequence of the equimolar cesium-to-lead ratio used for its preparation. Nevertheless, the NOESY spectrum of **NP20** (Fig. S7†) confirmed that its surface is passivated by oleic acid and decylamine, as indicated by the appearance of negative cross-peaks which can be attributed to the peculiar resonances of these two species.[51–53]

XRD patterns obtained in coupled ($\theta/2\theta$) scan mode are reported in Fig. 2I–L, and they clearly show the presence of preferred orientations (induced by the flat substrate on the anisotropic NCs), based on the comparison with the superimposed reference peak intensities. The last were confirmed by fitting the XRD patterns obtained at a small (5°) fixed incidence angle, showing more powder-like features and completeness of data (Fig. S8†). It should be noted that data in Fig. 2I–L were rescaled for graphical reasons, leading to a significant enhancement of the broad peak at around 20° for sample **NP20** (Fig. 2J); when normalizing all data to the collection time (not shown), it can be recognized that the scattering intensity of the amorphous component in sample **NP20** is only slightly larger than that in the other samples, while the intensity of the Bragg peaks is significantly smaller. The smaller diffraction intensity is likely affected by the preferred orientation of rods with their long axis parallel to the substrate plane, which implies that the intense reflections corresponding to a scattering vector oriented parallel to the long axis

of the rod can hardly fulfill the Bragg condition in $\theta/2\theta$ scan mode. The relative intensity of the broad peak is indeed reduced in the measurements at grazing incidence (Fig. S8†), where the Bragg peak around 15° is enhanced instead. The broad peak (~20°) evident in the XRD pattern of **NP20** and ascribed to a larger scattering contribution from the capping ligands is possibly due to unwashed organic residues found in the sample. A Le Bail whole-pattern fitting was performed by using the Rietveld program package QUANTO.[54,55] All samples were found to consist of a single crystalline phase: orthorhombic (*Pbnm*) $CsPbBr_3$ in the case of samples **NP6**, **NP20**, and **NP22** (cell parameters: a = 8.21 Å, b = 8.25 Å, c = 11.76 Å, and $\alpha = \beta = \gamma = 90°$), and trigonal Cs_4PbBr_6 ($R\bar{3}c$) in the case of sample **NP21** (cell parameters: $a = b$ = 13.73 Å, c = 17.32 Å, $\alpha = \beta = 90°$, and $\gamma = 120°$).

Concerning the morphologies of the NCs exhibiting near-unity PLQYs, it is apparent that what differentiated crystal evolution in our reactions is the suitable combination between the perovskite elements and the choice of the amine. Since attempts to slow down the crystallization rate could not be representative of the actual conditions generating highly luminescent NCs, a plausible reaction pathway could be deduced by comparing pre- and post-injection chemistry.

In the case of relatively low $C_6H_{13}Br$/PbO molar ratios (*i.e.*, the conditions leading to the formation of **NP6** nanocubes), we can admit that the nucleation of poorly coordinated bromoplumbate species could be competitive with the growth of square-shaped $[(RNH_3)_2PbBr_4]_n$ structures acting as templating agents (Fig. 3A). In the case of **NP6**, the intercalation of cesium into the small square-shaped $[(RNH_3)_2PbBr_4]_n$ structures does not interfere with the conventional nucleation stage on the final distribution of the symmetrical 3D cubes, being the dimensions of the templating agents comparable with those of the final nanoparticles (Fig. 3A). This reaction pathway is supported by the fact that $[(RNH_3)_2PbBr_4]_n$ structures are endowed with a peculiar absorption peak (λ = 395 nm), which makes them easily discernible by the optical characterization of the isolated NCs. In the absence of this absorption peak, one can conclude that the preformed $[(RNH_3)_2PbBr_4]_n$ structures are actually involved in the crystal formation acting as templating agents after the cesium injection step. The near-unity PLQY can be obtained for **NP6** as a result of the subtle interplay between the three perovskite elements, which avoids the introduction of structural defects during the fast nucleation and crystallization stages.

In the case of relatively high $C_6H_{13}Br$/PbO molar ratios, the rationalization of the reaction pathway leading to the final morphology of **NP20**, **NP21** and **NP22** must take into account the initial presence of large rod-like $[(RNH_3)_2PbBr_4]_n$ structures. In the case of **NP20**, it can reasonably be stated that its final morphology was consequent to the fragmentation and subsequent growth of $[(RNH_3)_2PbBr_4]_n$ structures, from which the nanorods molded their shapes (Fig. 3B). In fact, the observed nanorods in **NP20** were relatively smaller than the corresponding $[(RNH_3)_2PbBr_4]_n$ structures. Fragmentation should be promoted by the addition of Cs^+ ions to large two-dimensional structures, destabilizing them by partial removal of organic cations from their surface.[56] Under conditions in which the growth of $[(RNH_3)_2PbBr_4]_n$ structures was limited by the relatively low Cs/Pb molar ratios (for example **NP19**, Table S1†), the presence of residual large rod-like structures was spectroscopically detected (Fig. S5†) and was further confirmed by TEM investigations (Fig. S9†). While the organic shell governs the fragmentation process, the selective growth of new smaller rod-like structures occurred without the simultaneous nucleation of highly coordinated bromoplumbate species (prevalent at high $C_6H_{13}Br$/PbO molar ratios), which should lead to the concomitant formation of nanocubes. The scarce reactivity of highly coordinated bromoplumbate species towards cesium ion intercalation can be explained by considering their countercations (secondary ammonium ions, see top-left equations in Fig. 1) formed by the secondary amines which, being more basic than primary amines, sequestrate the protons generated by the SN_2 reactions during the incubation stage. Although not involved in the surface passivation of $CsPbBr_3$ NCs, the secondary ammonium ions tune the reactivity of bromoplumbate. The scarce reactivity of highly coordinated bromoplumbate species can therefore be rationalized by considering the high steric encumbrance of the secondary ammonium ions, hampering their nucleation.

In the presence of HAM at high $C_6H_{13}Br$/PbO molar ratios, large $[(RNH_3)_2PbBr_4]_n$ templating agents decompose into small square-shaped intermediate structures leading to the formation of nanocubes (Fig. 3C). It is reasonable to suppose that the stability of rod-like intermediate structures is severely compromised by the weaker inter-ligand interactions within their organic passivating shell, due to the shorter HAM chains with respect to their DAM counterparts, which, in contrast, sustain the existence of larger asymmetric two-dimensional structures in the course of the crystallization stage.

With this in mind, we can rationalize the production of cuboid shaped particles in the case of **NP22** with the growth of these generated small structures, while the evolution of Cs_4PbBr_6 rhombohedrons (selectively observed in the case of **NP21**) depends on the cesium-to-lead molar ratio. In fact, the lower steric encumbrance of HAM could promote the depletion of lead from the formed $CsPbBr_3$ NCs thus inducing the 3D → 0D transformation.[57] To substantiate our interpretation of the reaction mechanism at high $C_6H_{13}Br$/PbO molar ratios, we carried out TEM investigations also on a sample prepared in the presence of OAM (**NP8**, Table S1†). In this case (Fig. S10†), we observed the co-presence of nanocubes and nanorods, as a result of uncontrolled fragmentation of the preformed $[(RNH_3)_2PbBr_4]_n$ structures. Probably, the *cis*-configuration of the double bonds in OAM increases the free volume between the components of the organic shell, making the large rod-like growing structures unstable.

Next, we investigated the role of the ligand composition in the stability of the obtained near-unity PLQY NCs, which is the biggest issue afflicting colloidal all-inorganic perovskite nanoparticle dispersions when stored under ambient conditions. This drawback is due to the feeble NC surface passivation by

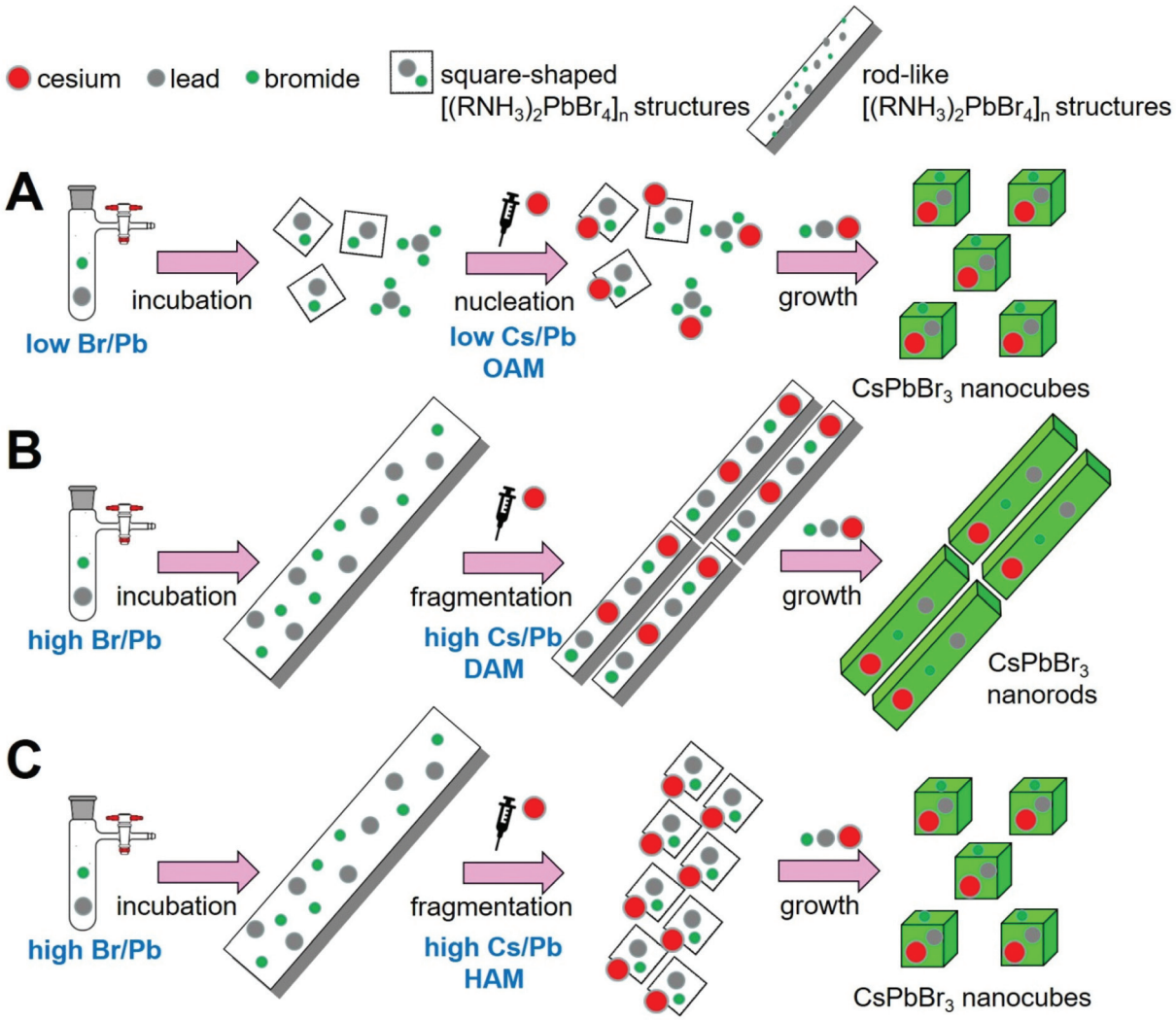

Fig. 3 Illustration of the proposed growth pathways leading to the formation of near-unity PLQY NCs under different conditions: (A) nanocubes obtained with low Br/Pb molar ratio (**NP6**); (B) nanorods obtained with high Br/Pb molar ratio (**NP20**); (C) nanocubes obtained with high Br/Pb molar ratio (**NP22**).

the organic ligands combined with the disaggregation of the perovskite ionic structure mainly induced by moisture. Therefore, we deemed it worthwhile to investigate the optical stability of our near-unity PLQY nanoparticles by measuring the PLQYs of their dispersions stored under ambient conditions as a function of time. As shown in Fig. 4, the PLQY behavior of the nanoparticles was monitored over 90 days, during which the dispersions retained their colloidal stability. However, **NP6** showed a significant drop in its emission efficiency (Fig. 4A), while the residual PLQY of **NP20** and **NP22** after 90 days was 98% in both cases (Fig. 4B and C). The lower optical stability exhibited by **NP6** resulted from the irreversible dissociation of oleylammonium bromide from the NC surface, which inevitably introduces halide vacancies within the pristine crystal lattice, thus reducing the initial PLQY. We suppose that the higher propensity towards the ligand decoordination at the organic/inorganic interface of **NP6** could be explained by the necessity of reducing the steric congestion within the organic shell passivating the NC surface. This tendency is more pronounced in the case of **NP6** than in the case of the other two perovskite NCs, due to the greater steric encumbrance of the longer chain amine (OAM).

Along with the long-term PLQY stability, the resistance against humidity was also ascertained for **NP20** and **NP22** by recording the time evolution of their emission spectra in a hexane/water (2/1 vol/vol) mixture, conditions greatly accelerating the moisture-induced perovskite decomposition. As shown in Fig. 4D, the green emission was maintained during the whole process in the case of **NP20**. Although the PL intensity gradually dropped, 76% of the initial PL intensity was retained after 24 hours, thus confirming the significant stability of **NP20**. In striking contrast, the green emission became very weak after 1 hour and completely disappeared in 24 hours for **NP22** (Fig. 4E). The higher hydrophobicity of the longer ali-

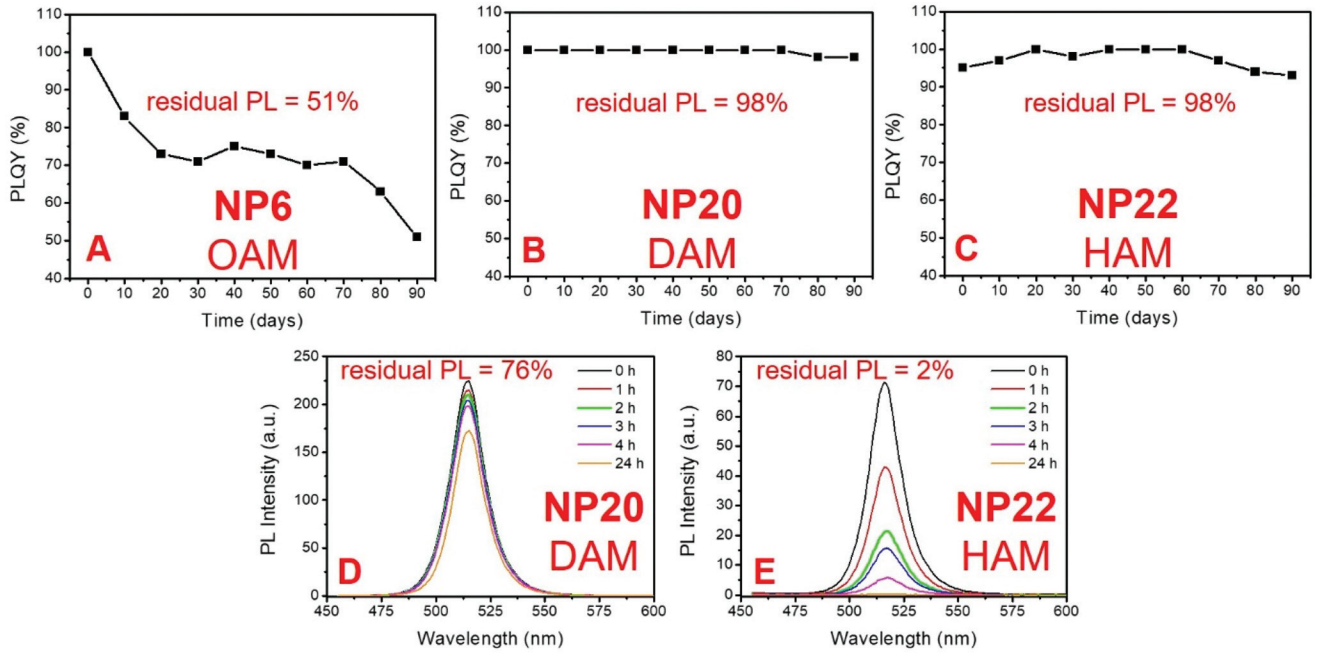

Fig. 4 PLQY trend as a function of time (days) for solutions in hexane of **NP6** (A), **NP20** (B) and **NP22** (C) stored under ambient conditions. PL spectra recorded in hexane/water (2/1 vol/vol) mixtures as aging tests for monitoring the emission properties of **NP20** (D) and **NP22** (E) in the presence of water.

phatic chain of DAM could be held responsible for the better resistance of **NP20** against the water-induced decomposition.

Conclusions

In this study, we proposed a conceptually original synthetic approach, in which a potentially controllable stage of the reaction anticipates the fast crystallization promoted by cesium injection. To make this possible, a mixture of lead oxide, 1-bromohexane (at different molar ratios with respect to lead) and the ligands (oleic acid and a suitable amine) in 1-octadecene was incubated for a period of 30 min before the injection of a warm cesium oleate solution. During this stage, the bromide ion release from reactions between the ligands and 1-bromohexane promoted the evolution of bromoplumbate species as well as two-dimensional $[(RNH_3)_2(PbBr_4)]_n$ structures with rod-like shapes at high $C_6H_{13}Br$/PbO molar ratios. The fine modulation of the reaction conditions permitted these preformed structures to act as templating agents for crystallization induced by cesium injection, ensuring, in the presence of decylamine, the direct formation of nanorods (aspect ratio ~10) endowed with near-unity PLQY. Under the other synthetic conditions systematically investigated in this study, near-unity PLQY nanocubes with different sizes were obtained by the simultaneous nucleation of individual bromoplumbate species (in the presence of oleylamine) or by decomposition of the preformed $[(RNH_3)_2(PbBr_4)]_n$ structures (in the presence of hexylamine). Furthermore, hexylamine also enabled to obtain the pure Cs_4PbBr_6 trigonal phase, which selectively emerged by using suitable Cs/Pb molar ratios, thus widening the scope of the proposed synthetic approach. The amine chain length exerted also an important role in the emission stability of the corresponding NCs, since only the nanocubes prepared in the presence of hexylamine maintained their PLQYs. In addition to the long-term stability (residual PLQY = 98% after 90 days under ambient conditions), the oleic acid/decylamine combination endowed the corresponding nanorods with a remarkable stability in contact with water, due to the hydrophobicity of the formed organic shell. These results could inspire the development of new synthetic methods for controlling the shape and stability of $CsPbBr_3$ NCs while maintaining their high emission efficiency.

Experimental section

Chemicals

Cesium carbonate (Cs_2CO_3, 99.9% metals basis, Alfa Aesar), lead oxide (PbO, 99.999% metals basis, Aldrich), 1-bromohexane (98%, Aldrich), oleylamine (OAM, technical grade 70%, Aldrich), decylamine (DAM, 95%, Aldrich), hexylamine (HAM, 99%, Aldrich) oleic acid (OLA, technical grade 90%, Aldrich), 1-octadecene (ODE, technical grade 90%, Aldrich), *n*-hexane (Aldrich, HPLC grade).

Synthesis of $CsPbBr_3$ NCs

The perovskite nanocrystal syntheses were performed under a nitrogen flow using standard Schlenk techniques. The cesium oleate solution was prepared as follows: Cs_2CO_3 (0.407 g,

1.25 mmol), OLA (1.55 mL, 4.91 mmol) and ODE (20 mL) were mixed in a 50 mL Schlenk tube and kept under vacuum for 1 hour at 120 °C; after the complete solubilization of the salt, the tube was filled with nitrogen and kept at 120 °C for the subsequent injection. To a 50 mL Schlenk tube, ODE (7.5 mL), lead oxide (85.2 mg, 0.g, 0.38 mmol), oleic acid (1.0 mL), amine (3.0 mmol) and 1-bromohexane (160, 213, 266 or 320 μl) were added and the mixture was heated at 160 °C. A complete solubilization of the reactants was observed within 5 min followed by the formation of a white precipitate. The reaction was prolonged for 30 min at constant temperature, followed by injection of the Cs-oleate solution (0.8–3.2 mL). After 10 s, the reaction mixture was cooled in an ice bath. The crude solution was centrifuged at 4000 rpm for 40 min. The supernatant containing unreacted precursors was discarded and the obtained precipitate was dispersed in hexane (1.2 mL).

Isolation of $[(RNH_3)_2(PbBr_4)]_n$ structures

ODE (7.5 mL), lead oxide (85.2 mg, 0.g, 0.38 mmol), oleic acid (1.0 mL), oleylamine (1.0 mL) and 1-bromohexane (160, 213, 266 or 320 μl) were added to a 50 mL Schlenk tube and the mixture was heated at 160 °C. After 30 min, the mixture was cooled in an ice/water bath, centrifuged and the obtained precipitate was dissolved in hexane for the morphological characterization. The course of the reaction carried out with the lowest $C_6H_{13}Br$/PbO ratio was spectroscopically monitored by sampling small aliquots of the mixture at specified reaction times and dissolving them in hexane for further analysis.

Optical characterization

UV–vis absorption spectra were obtained using a Jasco V670 spectrometer operated in transmission mode. The absorption spectra were recorded for NC solutions exhibiting a relatively low absorbance (~0.1) at the excitonic peak. Steady-state photoluminescence (PL) spectra of the same solutions were acquired using a Varian Cary Eclipse instrument. The quantum yields were determined by using fluorescein as the standard, according to the literature procedures.[58]

Transmission electron microscopy (TEM) characterization

TEM micrographs were taken using a JEOL JEM1011 microscope, operating at an accelerating voltage of 100 kV. The instrument was equipped with a tungsten electron source, and a high-resolution CCD camera. Samples for TEM analysis were prepared by dipping the carbon-coated copper grid into the NC cyclohexane solution diluted with anhydrous *n*-hexane. Statistical size analysis (NC average size and standard deviation) was performed by using a freeware image analysis application (AxioVision); sizes of not less than one hundred nanoparticles were measured for each sample.

FEG-SEM-EDX

Elemental analyses were performed using a field emission gun scanning electron microscope (FEG-SEM) Zeiss Σigma 300 VP (Zeiss Oberkochen, Germany) equipped with an energy dispersive spectrometer (EDX) C-MaxN SDD with an active area of 20 mm^2 (Oxford Instruments, Oxford, United Kingdom). NC solutions in cyclohexane were deposited on aluminum stubs coated with a pure graphite tape. Analysis was carried out at 15 kV using a 7.5 mm working distance at a 1000× magnification. The data accuracy was checked against standards by MAC (Micro-Analysis Consultants Ltd, United Kingdom).

X-ray diffraction

XRD data were collected both in coupled sample-detector (θ/2θ) scan mode and in detector (2θ) scan mode at a 5° incidence angle, by using a Bruker D8 Discover equipped with a Cu source (Kα line), a Göbel mirror, and a scintillation point detector.

Nuclear magnetic resonance

^{1}H-NMR spectra were recorded on a Varian 500 MHz spectrometer. All chemical shifts were referred to the non-deuterated benzene residue signal at δ 7.16 ppm. The nuclear Overhauser effect spectroscopy (NOESY) spectra were acquired using a 300 ms mixing time.

Conflicts of interest

There are no conflicts to declare.

Acknowledgements

Regione Puglia (INNOLABS project DEMETRA – COD. Y8V9H90-1) is gratefully acknowledged for funding.

References

1 B. R. Sutherland and E. H. Sargent, *Nat. Photonics*, 2016, **10**, 295–302.
2 K. Lin, J. Xing, L. N. Quan, F. P. G. de Arquer, X. Gong, J. Lu, L. Xie, W. Zhao, D. Zhang, C. Yan, W. Li, X. Liu, Y. Lu, J. Kirman, E. H. Sargent, Q. Xiong and Z. Wei, *Nature*, 2018, **562**, 245–248.
3 W. S. Yang, B.-W. Park, E. H. Jung, N. J. Jeon, Y. C. Kim, D. U. Lee, S. S. Shin, J. Seo, E. K. Kim, J. H. Noh and S. I. Seok, *Science*, 2017, **356**, 1376–1379.
4 L. Protesescu, S. Yakunin, M. I. Bodnarchuk, F. Krieg, R. Caputo, C. H. Hendon, R. X. Yang, A. Walsh and M. V. Kovalenko, *Nano Lett.*, 2015, **15**, 3692–3696.
5 J. Shamsi, A. S. Urban, M. Imran, L. De Trizio and L. Manna, *Chem. Rev.*, 2019, **119**, 3296–3348.
6 J. Kang and L. Wang, *J. Phys. Chem. Lett.*, 2017, **8**, 489–493.
7 M. I. Bodnarchuk, S. C. Boehme, S. ten Brinck, C. Bernasconi, Y. Shynkarenko, F. Krieg, R. Widmer, B. Aeschlimann, D. Gunther, M. V. Kovalenko and I. Infante, *ACS Energy Lett.*, 2019, **4**, 63–74.
8 D. Yang, X. Li and H. Zeng, *Adv. Mater. Interfaces*, 2018, **5**, 1701662.

9 J. De Roo, M. Ibáñez, P. Geiregat, G. Nedelcu, W. Walravens, J. Maes, J. C. Martins, I. Van Driessche, M. V. Kovalenko and Z. Hens, *ACS Nano*, 2016, **10**, 2071–2081.

10 R. Grisorio, M. E. Di Clemente, E. Fanizza, I. Allegretta, D. Altamura, M. Striccoli, R. Terzano, C. Giannini, M. Irimia-Vladu and G. P. Suranna, *Nanoscale*, 2019, **11**, 986–999.

11 E. Fanizza, F. Cascella, D. Altamura, C. Giannini, A. Panniello, L. Triggiani, F. Panzarea, N. Depalo, R. Grisorio, G. P. Suranna, A. Agostiano, M. L. Curri and M. Striccoli, *Nano Res.*, 2019, **12**, 1155–1166.

12 R. Grisorio, E. Fanizza, I. Allegretta, D. Altamura, M. Striccoli, R. Terzano, C. Giannini, V. Vergaro, G. Ciccarella, N. Margiotta and G. P. Suranna, *Nanoscale*, 2020, **12**, 623–637.

13 J. Pan, Y. Shang, J. Yin, M. De Bastiani, W. Peng, I. Dursun, L. Sinatra, A. M. El-Zohry, M. N. Hedhili, A.-H. Emwas, O. F. Mohammed, Z. Ning and O. M. Bakr, *J. Am. Chem. Soc.*, 2018, **140**, 562–565.

14 Y. Wu, X. Li and H. Zeng, *ACS Energy Lett.*, 2019, **4**, 673–681.

15 J. Kang and L. Wang, *J. Phys. Chem. Lett.*, 2017, **8**, 489–493.

16 S. Sun, D. Yuan, Y. Xu, A. Wang and Z. Deng, *ACS Nano*, 2016, **10**, 3648–3657.

17 A. Pan, B. He, X. Fan, Z. Liu, J. J. Urban, A. P. Alivisatos, L. He and Y. Liu, *ACS Nano*, 2016, **10**, 7943–7954.

18 S. Paul and A. Samanta, *ACS Energy Lett.*, 2020, **5**, 64–69.

19 M. Imran, V. Caligiuri, M. Wang, L. Goldoni, M. Prato, R. Krahne, L. De Trizio and L. Manna, *J. Am. Chem. Soc.*, 2018, **140**, 2656–2664.

20 C. Sun, Z. Gao, H. Liu, C. Geng, H. Wu, X. Zhang, C. Fan and W. Bi, *Dalton Trans.*, 2018, **47**, 16218–16224.

21 F. Krieg, S. T. Ochsenbein, S. Yakunin, S. ten Brinck, P. Aellen, A. Süess, B. Clerc, D. Guggisberg, O. Nazarenko, Y. Shynkarenko, S. Kumar, C.-J. Shih, I. Infante and M. V. Kovalenko, *ACS Energy Lett.*, 2018, **3**, 641–646.

22 A. Dutta, R. K. Behera, P. Pal, S. Baitalik and N. Pradhan, *Angew. Chem., Int. Ed.*, 2019, **58**, 5552–5556.

23 A. Dutta, S. K. Dutta, S. Das Adhikari and N. Pradhan, *ACS Energy Lett.*, 2018, **3**, 329–334.

24 T. Chen, Y. Xu, Z. Xie, W. Jiang, L. Wang and W. Jiang, *Nanoscale*, 2020, **12**, 9569–9580.

25 M. I. Bodnarchuk, S. C. Boehme, S. ten Brinck, C. Bernasconi, Y. Shynkarenko, F. Krieg, R. Widmer, B. Aeschlimann, D. Günther, M. V. Kovalenko and I. Infante, *ACS Energy Lett.*, 2019, **4**, 63–74.

26 D. P. Nenon, K. Pressler, J. Kang, B. A. Koscher, J. H. Olshansky, W. T. Osowiecki, M. A. Koc, L.-W. Wang and A. P. Alivisatos, *J. Am. Chem. Soc.*, 2018, **140**, 17760–17772.

27 R. Grisorio, E. Fanizza, M. Striccoli, D. Altamura, C. Giannini, I. Allegretta, R. Terzano and G. P. Suranna, *ChemNanoMat*, 2020, **6**, 356–361.

28 Y. Tong, B. J. Bohn, E. Bladt, K. Wang, P. Mueller-Buschbaum, S. Bals, A. S. Urban, L. Polavarapu and J. Feldmann, *Angew. Chem., Int. Ed.*, 2017, **56**, 13887–13892.

29 Y. Li, H. Huang, Y. Xiong, A. F. Richter, S. V. Kershaw, J. Feldmann and A. L. Rogach, *ACS Nano*, 2019, **7**, 8237–8245.

30 L. Peng, A. Dutta, R. Xie, W. Yang and N. Pradhan, *ACS Energy Lett.*, 2018, **3**, 2014–2020.

31 Y. Li, H. Huang, Y. Xiong, S. V. Kershaw and A. L. Rogach, *Angew. Chem., Int. Ed.*, 2018, **57**, 5833–5837.

32 Q. Jing, Y. Su, X. Xing and Z. Lu, *J. Mater. Chem. C*, 2019, **7**, 1854–1858.

33 C. Lu, M. W. Wright, X. Ma, H. Li, D. S. Itanze, J. A. Carter, C. A. Hewitt, G. L. Donati, D. L. Carroll, P. M. Lundin and S. M. Geyer, *Chem. Mater.*, 2019, **31**, 62–67.

34 J.-R. Wen, B. J. Roman, F. A. Rodriguez Ortiz, N. Mireles Villegas, N. Porcellino and M. Sheldon, *Chem. Mater.*, 2019, **31**, 8551–8557.

35 G. Almeida, O. J. Ashton, L. Goldoni, D. Maggioni, U. Petralanda, N. Mishra, Q. A. Akkerman, I. Infante, H. J. Snaith and L. Manna, *J. Am. Chem. Soc.*, 2018, **140**, 14878–14886.

36 M. Imran, P. Ijaz, D. Baranov, L. Goldoni, U. Petralanda, Q. Akkerman, A. L. Abdelhady, M. Prato, P. Bianchini, I. Infante and L. Manna, *Nano Lett.*, 2018, **18**, 7822–7831.

37 J. S. Manser, M. I. Saidaminov, J. A. Christians, O. M. Bakr and P. V. Kamat, *Acc. Chem. Res.*, 2016, **49**, 330–338.

38 S. J. Yoon, K. G. Stamplecoskie and P. V. Kamat, *J. Phys. Chem. Lett.*, 2016, **7**, 1368–1373.

39 Y. Zhang, M. I. Saidaminov, I. Dursun, H. Yang, B. Murali, E. Alarousu, E. Yengel, B. A. Alshankiti, O. M. Bakr and O. F. Mohammed, *J. Phys. Chem. Lett.*, 2017, **8**, 961–965.

40 G. Almeida, L. Goldoni, Q. Akkerman, Z. Dang, A. H. Khan, S. Marras, I. Moreels and L. Manna, *ACS Nano*, 2018, **12**, 1704–1711.

41 M. P. U. Haris, R. Bakthavatsalam, S. Shaikh, B. P. Kore, D. Moghe, R. G. Gonnade, D. D. Sarma, D. Kabra and J. Kundu, *Inorg. Chem.*, 2018, **57**, 13443–13452.

42 N. T. K. Thanh, N. Maclean and S. Mahiddine, *Chem. Rev.*, 2014, **114**, 7610–7630.

43 Q. A. Akkerman, S. Park, E. Radicchi, F. Nunzi, E. Mosconi, F. De Angelis, R. Brescia, P. Rastogi, M. Prato and L. Manna, *Nano Lett.*, 2017, **17**, 1924–1930.

44 G. Nedelcu, L. Protesescu, S. Yakunin, M. I. Bodnarchuk, M. J. Grotevent and M. V. Kovalenko, *Nano Lett.*, 2015, **15**, 5635–5640.

45 S. ten Brinck and I. Infante, *ACS Energy Lett.*, 2016, **1**, 1266–1272.

46 J. A. Sichert, Y. Tong, N. Mutz, M. Vollmer, S. Fischer, K. Z. Milowska, R. García Cortadella, B. Nickel, C. Cardenas-Daw, J. K. Stolarczyk, A. S. Urban and J. Feldmann, *Nano Lett.*, 2015, **15**, 6521–6527.

47 V. K. Ravi, P. K. Santra, N. Joshi, J. Chugh, S. K. Singh, H. Rensmo, P. Ghosh and A. Nag, *J. Phys. Chem. Lett.*, 2017, **8**, 4988–4994.

48 M. V. Kovalenko, L. Protesescu and M. I. Bodnarchuk, *Science*, 2017, **358**, 745–750.
49 B. Zhang, L. Goldoni, J. Zito, Z. Dang, G. Almeida, F. Zaccaria, J. de Wit, I. Infante, L. De Trizio and L. Manna, *Chem. Mater.*, 2019, **31**, 9140–9147.
50 Q. Zhong, M. Cao, Y. Xu, P. Li, Y. Zhang, H. Hu, D. Yang, Y. Xu, L. Wang, Y. Li, X. Zhang and Q. Zhang, *Nano Lett.*, 2019, **19**, 4151–4157.
51 Z. Hens and J. C. Martins, *Chem. Mater.*, 2013, **25**, 1211–1221.
52 R. Grisorio, D. Debellis, G. P. Suranna, G. Gigli and C. Giansante, *Angew. Chem., Int. Ed.*, 2016, **55**, 6628–6633.
53 D. Quarta, M. Imran, A.-L. Capodilupo, U. Petralanda, B. Van Beek, F. De Angelis, L. Manna, I. Infante, L. De Trizio and C. Giansante, *J. Phys. Chem. Lett.*, 2019, **10**, 3715–3726.
54 A. Altomare, M. C. Burla, C. Giacovazzo, A. Guagliardi, A. G. G. Moliterni, G. Polidori and R. Rizzi, *J. Appl. Crystallogr.*, 2001, **34**, 392–397.
55 A. Le Bail, H. Duroy and J. L. Fourquet, *Math. Res. Bull.*, 1988, **23**, 447–452.
56 S. D. Adhikari, A. Dutta, S. K. Dutta and N. Pradhan, *ACS Energy Lett.*, 2018, **3**, 1247–1253.
57 F. Palazon, G. Almeida, Q. A. Akkerman, L. De Trizio, Z. Dang, M. Prato and L. Manna, *Chem. Mater.*, 2017, **29**, 4167–4171.
58 M. Grabolle, M. Spieles, V. Lesnyak, N. Gaponik, A. Eychmüller and U. Resch-Genger, *Anal. Chem.*, 2009, **81**, 6285–6294.